Supporting Information

Tarasov et al. 10.1073/pnas.1014598108

SI Methods

In Vitro Toxicity Assay. MDA-MB-231 cells were obtained from American Type Cell Culture Collection. Cells were grown in RPMI medium 1640 supplemented with 10% fetal bovine serum (FBS). For the assay, cells were seeded into 96-well plates in medium containing 5% FBS and 100 μL of a cell suspension containing 5,000 cells per well were used for each well. After 1 d incubation, the 5% FBS medium was aspirated and replaced with 100 μL of serum-free RPMI medium 1640 containing 1 mg bovine serum albumin (BSA) per 1 mL RPMI medium 1640. The compounds were prepared to the desired dilutions in no serum medium containing 1 mg BSA/mL. 75 μL of compounds were added to the wells followed by addition of 25 μL of human recombinant SDF-1α (Peprotech) to attain final concentrations of 10 ng SDF-1α / mL medium. Cell growth was evaluated utilizing MTT ((3-(4,5-Dimethylthiazol-2-yl)-2,5-diphenyltetrazolium bromide). The absorbance of the wells at 544 nm was determined by a FLUOstar/POLARstar Galaxy (BMG Lab Technologies GmbH) microplate reader. The activity was calculated from the data using the formula: $100 \times [(T - T_0)/(C - T_0)]$ for $T > T_0$ and $100 \times [(T - T_0)/T_0]$ for $T < T_0$. T_0 corresponds to cell density at the time of compound addition and C is the density of untreated cells.

Transmission Electron Microscopy. Two microliters of a sample was applied directly on a microscopy grid, air-dried, stained with 0.5% (w/v) uranyl acetate, and visualized using either a Tecnai 12 transmission electron microscope (FEI Company, OR) or a Hitachi H-7000 electron microscope equipped with a digital camera system (Gatan, Inc.).

CD Spectroscopy. The CD spectra of peptide solutions (12–50 μM) in 1 or 0.2 mm path-length quartz cuvettes were recorded at 25 °C using Aviv 202 Series CD-spectrometer (Aviv Biomedicals, Inc.) at the wavelength interval 260–180 nm. The intensity measurements were made every 0.5 nm with data collection interval at least 5 s.

NMR Spectroscopy. The peptides were dissolved in DMSO-d_6 and the final concentration was approximately 1 mM. The ^{13}C-edited heteronuclear single quantum coherence (HSQC), total correlation spectroscopy (TOCSY), and NOESY experiments were carried out on Varian 600 MHz and Bruker Avance 600 MHz spectrometers at 298 K. Mixing times for TOCSY and NOESY were 30 and 500 ms, respectively. All NMR data were processed with the nmrPipe program package (1). The zero-filling and sine-bell window function was applied to both direct and indirect dimensions prior to Fourier transformation. A linear prediction was applied to the data in the indirect dimension. The Sparky program was used for data analysis (http://www.cgl.ucsf.edu/home/sparky/). NOEs and dihedral angles were used for structure calculations. NOEs were classified as strong, medium, or weak corresponding to distance restraints of 1.8–2.5, 2.5–3.5, 3.5–6.0, and 3,5–7.0 Å (for methyl NOEs), respectively. The distance restraints were derived from cross-peak volumes calibrated against the Hε-Hζ interproton distance (2.45 Å) of Trp18. Dihedral angle restraints were acquired from the analysis of the chemical shift index for $^{13}C_\alpha$ and $^{13}C_\beta$ using TALOS software (2). The initial 100 structures were generated using CNS 1.1 (http://cns-online.org/v1.21/). Twenty structures with the lowest energy, showing least violation of restraints, were selected among initial structures. The structure analysis was carried out using MOLMOL (3) to identify violations of NOE and dihedral angle restraints and to superimpose structures and measure rmsd.

Characterization of Drug Encapsulation by Fluorescence Spectroscopy. The fluorescence emission spectra were obtained at 25 °C on a Fluoromax-2 single-photon counting spectrofluorometer from Horiba Jobin-Ivon, Inc. The excitation and emission monochromator slits were 1.5–3 and 3.5–7 nm, respectively. The solutions of peptides were prepared in the same manner as for the light scattering studies. The 20 μM stock solutions of imidazoacridone WMC77 ["2c"(4)] were prepared in deionized water. Probes with different peptide concentrations and/or peptide/imidazoacridone ratios were prepared by adding aliquots of one component to the solution of another. The final imidazoacridone concentration for all solutions was 300 nM.

Laser Scanning Confocal Microscopy. Cells have been grown in cover glass bottom petri dishes (MatTek Corp.). The images were collected on Olympus fluoview FV1000 spinning disk confocal microscope using a 40 × /1.3 oil immersion objective. For membrane labeling, cells were treated with 5 μg/mL solution of the lipophilic carbocyanine dye DiOC18 (3) (Invitrogen) for 30 min at 37 °C and rinsed with PBS three times. Nanoparticles formed by rhodamine red -labeled X4-2-1 were added to the cells and cell entry was observed in real time by scanning with 1 min intervals at room temperature. After 20 min of observation, cells were rinsed with PBS and Z-stack images of green and red fluorescence were acquired simultaneously using the acquisition time between 0.3 and 1.0 s to minimize the effects of intracellular movements. The fluorescence of DiOC18 (3) and rhodamine was excited using the 488 nm band of Multi Ar laser and the 543 nm band of a HeNe laser, respectively. The emission was detected using a 505–525 nm filter for DiOC18 (3) and a 560–660 nm filter for rhodamine. The 3D images were built using ImageJ (1.43u, Wayne Rasband, National Institute of Health).

Animal Studies. The 10^6 MDA-MB-231 breast cancer cells have been injected intravenously into 4-week-old (20–22 g) female athymic Ncr-nu/nu mice (Animal Production Area of the National Cancer Institute). The mice were divided into three groups, five mice in each group and the treatment was initiated the following day after injection of tumor cells. The control group received phosphate buffered saline solution intraperitoneally once every 3 d. Two other groups were treated once every 3 d with 200 μL of either 0.3 mg/mL (3 mg/kg dose) or 1.2 mg/mL (12 mg/kg dose) X4-2-6 solution in PBS containing 1.25% (v/v) DMSO. Animal care was provided in accordance with the procedures outlined in ref. 5.

1. Delaglio F, et al. (1995) NMRPipe: A multidimensional spectral processing system based on UNIX pipes. *J Biomol NMR* 6:277–293.
2. Cornilescu G, Delaglio F, Bax A (1999) Protein backbone angle restraints from searching a database for chemical shift and sequence homology. *J Biomol NMR* 13:289–302.
3. Koradi R, Billeter M, Wuthrich K (1996) MOLMOL: A program for display and analysis of macromolecular structures.*J Mol Graph* 14:51–32.
4. Tarasov SG, Casas-Finet JR, Cholody WM, Michejda CJ (1999) Bisimidazoacridones: effect of molecular environment on conformation and photophysical properties. *Photochem Photobiol* 70:568–578.
5. National Research Council. (1996) *Guide for Care and Use of Laboratory Animals* (National Academy Press, Washington, DC).

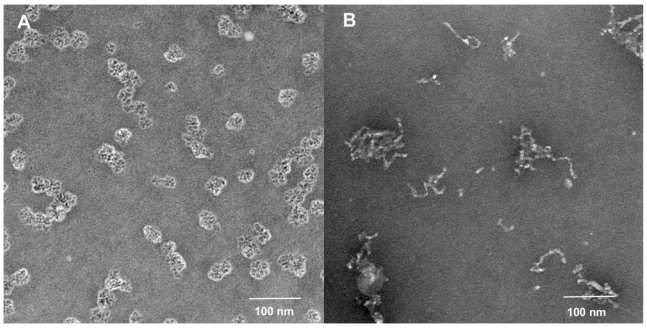

Fig. S1. Nanoparticles formed by different transmembrane peptides form super aggregates of different shapes and sizes. Transmission electron microscopy of self-assembled nanoparticles. (*A*) Inhibitor of P-glycoprotein derived from the second transmembrane helix, MDR1-2-2 (DDTRYAYYYSGIGAGVLVAAYIQVS) (1), (*B*) Inhibitor of P-glycoprotein derived from the fifth transmembrane helix, MDR1-5-4 (LIYASYALAFWYGTTLVLSGEGSDD).

1 Tarasova NI, et al. (2005) Transmembrane inhibitors of P-glycoprotein, an ABC transporter. *J Med Chem* 48:3768–3775.

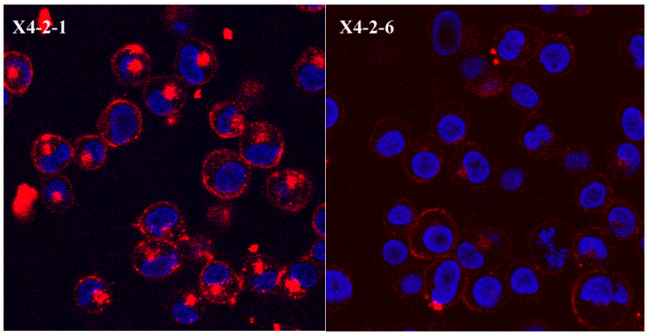

Fig. S2. Extended polyethylenglycol tails interfere with membrane fusion and cell entry of self-assembling fusogenic protoviral nanoparticles. MDA-MB-231 breast cancer cells were treated with nanoparticles generated from a mixture of either X4-2-1 or X4-2-6 with X4-2-6 peptide labeled with Alexa680. The ratio of nonlabeled to labeled peptide in nanoparticles was 10:1. X4-2-1 peptide (LLFVITLPFWAVDAVANWYFGNDD) had no PEG, whereas X4-2-6 was modified with PEG containing 27 monomeric units (FVITLPFWAVDAVANWYFGNDD-$(CH_2CH_2O)_{27}$-NH_2). The cells were exposed to nanoparticles for 30 min at 37 °C, rinsed with medium and incubated for 5 min with 50 μM Hoechst 33342. The images were collected on a Zeiss LSM510 laser scanning confocal microscope using a 40 × /1.3 oil immersion objective lens. The red color represents fluorescence of Alexa-680 of the peptide and the blue color reflects Hoechst 33342. The fluorescence of Alexa680 was excited using the 633 nm band of a HeNe laser and recorded using the 660–740 nm emission filter. The fluorescence of Hoechst 33342 complexed to DNA was excited using the 780 nm band of a Titanium Sapphire laser, and recorded using a 390–465 nm filter.

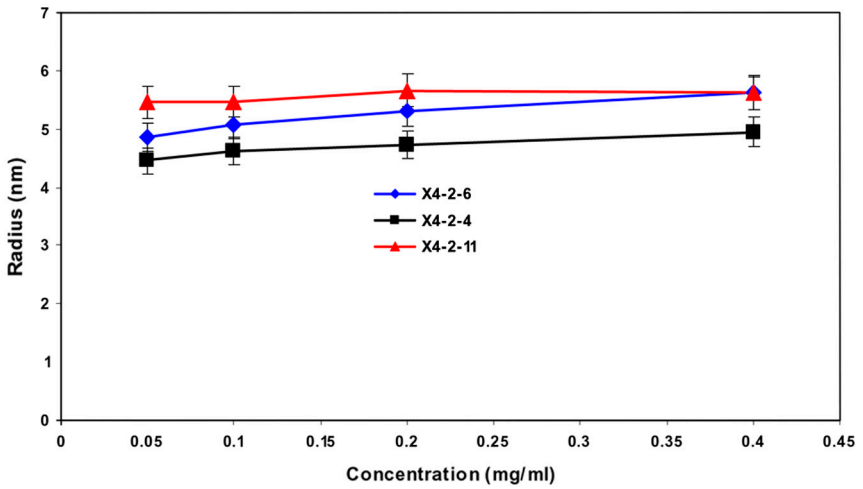

Fig. S3. The size of the nanoparticles was independent of peptide concentration in 0.05–0.4 mg/mL range. The radii were determined by dynamic light scattering (DLS). The peptide solutions in PBS buffer, pH 7.2 were prepared from 32 mg/mL stock solutions of peptides in DMSO. The final concentration of DMSO in all samples was 1.25% (v/v). The solutions were sonicated for 10 min and left at ambient temperature overnight (about 20 h before the measurements). Next day, the samples were spun at 15,000 g for 10 min to remove dust and particular impurities and analyzed by DLS on DynaPro Titan instrument equipped with a Temperature-Controlled MicroSampler (Wyatt Technology Corp.) at a laser wavelength of 830 nm. Seventy microliters of each sample was placed in a quartz cuvette. Each measurement consisted of ten 10- or 20-second acquisitions. The DLS measurements were carried out at a scattering angle of 90°. To obtain the hydrodynamic radii (R_h), the intensity autocorrelation functions were analyzed by "Dynamics 6.7.7.9." software (Wyatt Technology Corp.). For data analysis, a viscosity and refractive index values for the solution of 1.25% DMSO in water (v/v) were calculated using data from (1). Results from different measurements of the same sample were averaged and standard deviation was calculated.

1 Nieto-Draghi C, Avalos JB, Rousseau B (2003) Transport properties of dimethyl sulfoxide aqueous solutions. *J Chem Phys* 119:4782–4789.

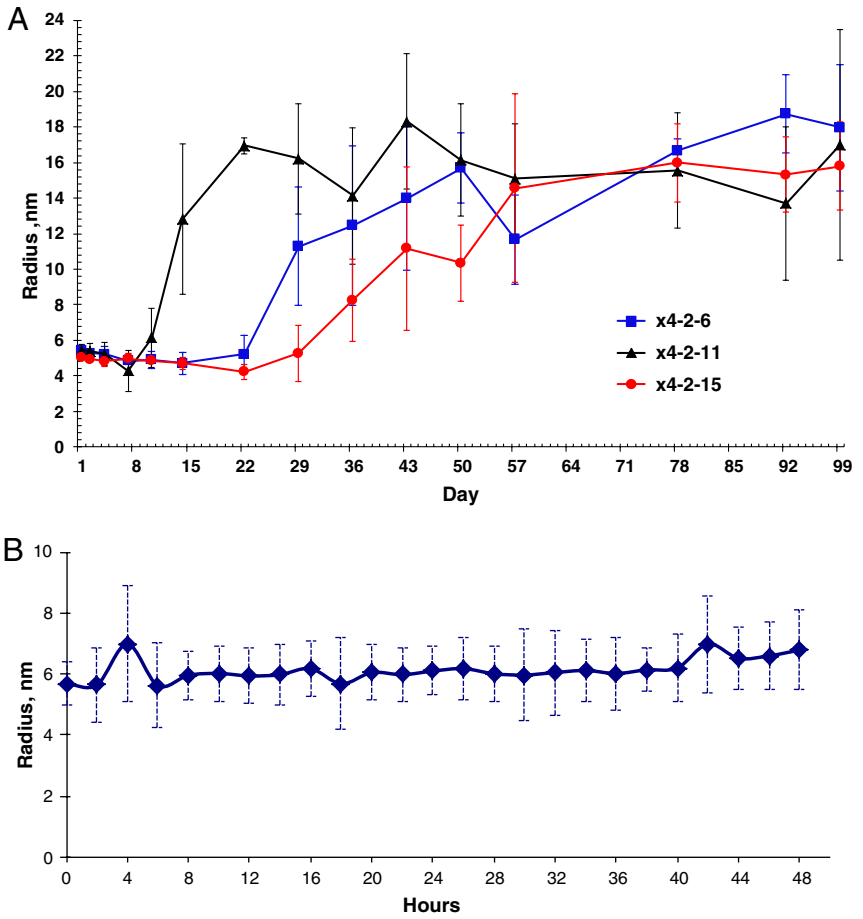

Fig. S4. Structural stability of nanoparticles as a function of time. The radii and size distributions were determined by dynamic light scattering for 0.4 mg/mL solutions of peptides in PBS containing 1.25% (v/v) DMSO as described in the legend to Fig. S3. (*A*) Stability upon incubation at room temperature; (*B*) Stability of X4-2-6 nanoparticles at 37 °C.

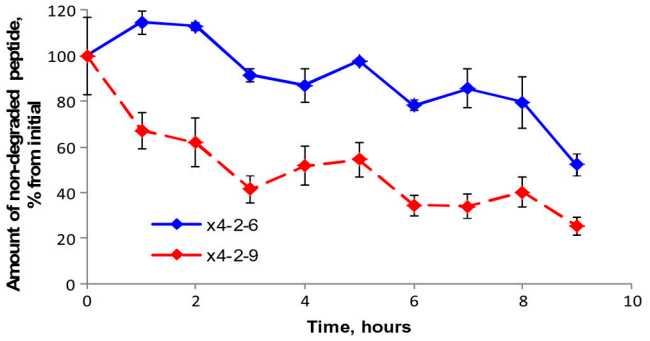

Fig. S5. Determination of self-assembling peptide stability against proteolytic degradation. We incubated 2 mg/mL of X4-2-6 nanospheres and X4-2-9 fibrils in bovine serum. Equal 50 μL aliquots were taken every hour during incubation and assayed on a coupled Xcalibur HPLC-MS system. The peptide molecular weight was determined using mass spectrometry, whereas 280 nm absorbance was measured by an HPLC UV detector. The extinction coefficients of X4-2-6 and X4-2-9 at 280 nm are identical and are equal to 12,660. A Shimadzu Prominence HPLC system with UV/Vis photodiode array detector was used for analysis of peptide degradation. A Shimadzu C18 reverse-phase column (50 mm × 4.5 mm) was equilibrated with 0.1% trifluoroacetic acid (TFA). The sample injection volume was 5 μL. The peptide was eluted with a linear gradient of 90% acetonitrile containing 0.1% TFA. The amount of nondegraded peptide was estimated by measuring peak area at 280 nm.

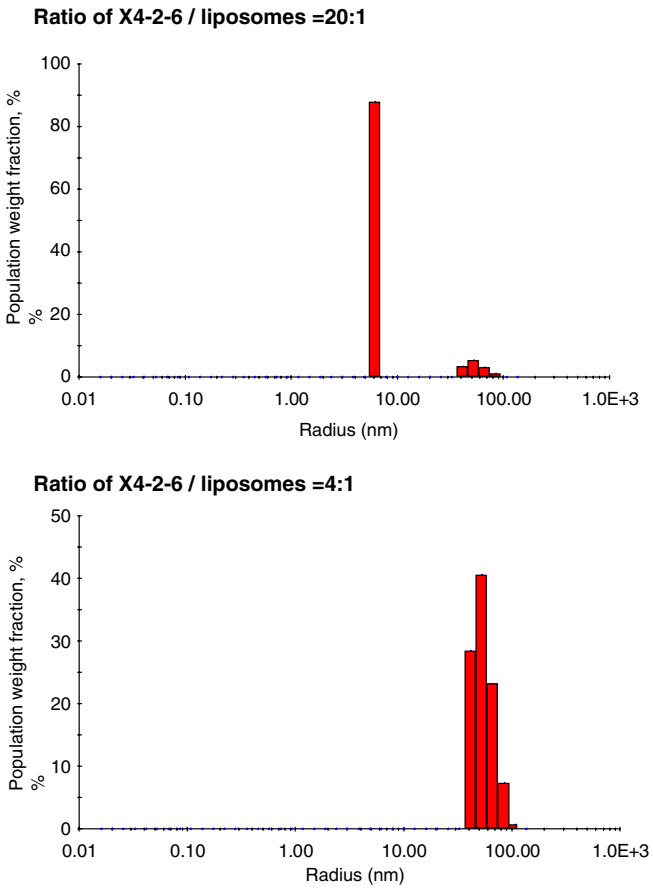

Fig. S6. Fusion of self-assembling nanoparticles with a lipid bilayer was observed by dynamic light scattering (DLS). X4-2-6 nanoparticles, 0.2 mg/mL in phosphate buffered saline have been titrated with 1,2-dioleoyl-*sn*-glycero-3-phosphocholine (DOPC)/1,2-dioleoyl-*sn*-glycero-3-phospho-(1′-*rac*-glycerol) (DOPG)/cholesterol liposomes (HTD Biosystems Inc.). The X4-2-6 nanoparticles (radius approximately 5.5 nm) could be easily detected in the presence of small amounts of liposomes (radius of approximately 55 nm) (*Upper*), whereas increase in liposome concentration results in complete elimination of "free" nanoparticles (*Lower*). The samples have been analyzed on DynaPro Titan instrument as described in the legend to Fig. S3.

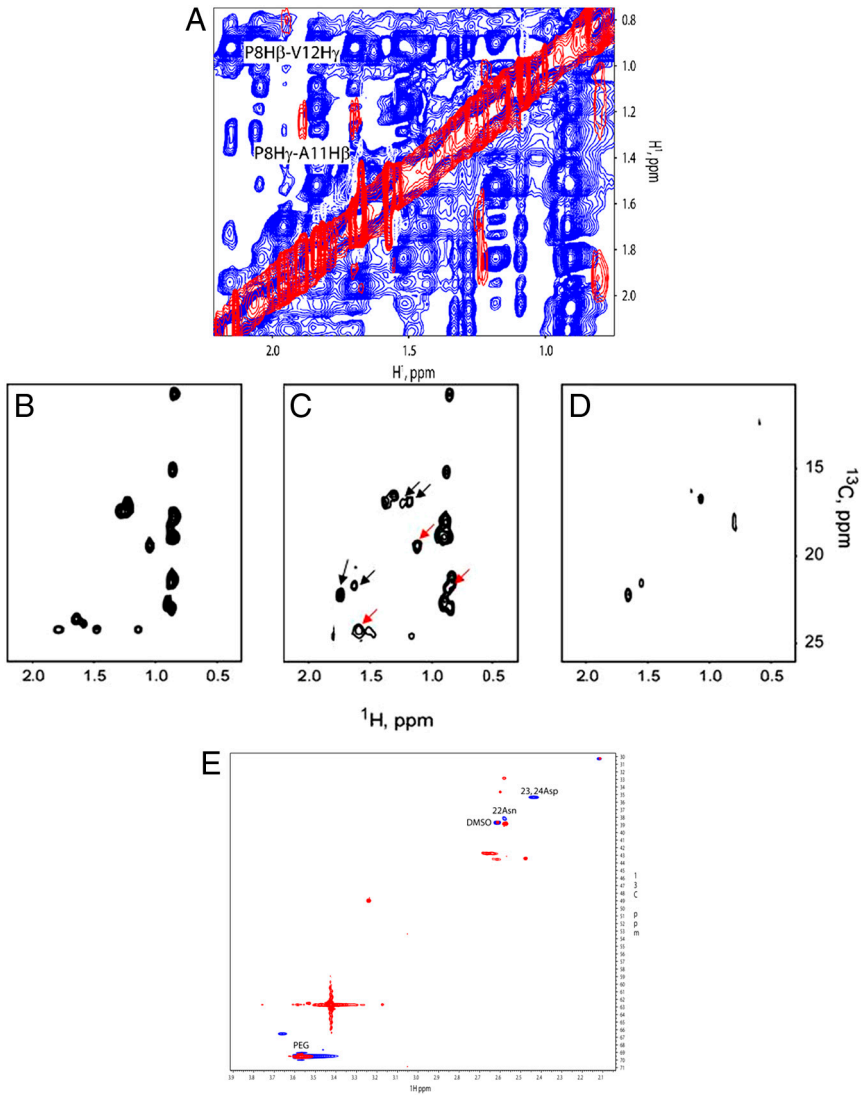

Fig. S7. NMR spectroscopy of X4-2-1and X4-2-6. (*A*) Overlay of 500 ms NOESY spectra of X4-2-1 in DMSO (blue) and in PBS (red). The marked signals show NOEs between P8 and V12 and P8 and A11 in DMSO and in PBS. The signal assignments for X4-2-1 in PBS were carried out using DMSO titration experiments. Preservation of NOEs in the head of the X4-2-1 hairpin region upon peptide transfer into PBS indicates that the hairpin topology observed in monomeric X4-2-1 in DMSO also exists when the peptide is assembled into nanoparticles in PBS. The spectra were acquired at 600 MHz (in DMSO) and at 900 MHz (in PBS) at 25 °C with 512 indirect points and processed using NMRPipe software. (*B–D*) ^{13}C HSQC spectra showing the methyl regions of X4-2-1 in (*B*) 100% DMSO, (*C*) 50% DMSO, (*D*) aqueous solution. Black arrows in (*C*) mark resonances in slow exchange and red arrows mark Thr6 and Leu7 resonances in intermediate exchange that are reporting on intermolecular contacts mediating nanoparticle assembly. (*E*) ^{13}C HSQC comparison of x4-2-6 nanoparticles in PBS (blue) with x4-2-6 nanoparticles in the presence of cell membrane preparation (EMD Millipore) (red). The spectra were acquired on a 900 MHz Bruker spectrometer at 25 °C. Most peptide signals are broadened beyond detection due to the high molecular weight of the peptide assembly. Only the signals belonging to the PEG moiety and to Asn 22, Asp 23, and Asp24 were observed. These assignments were confirmed using chemical shift perturbations caused by DMSO titration. The C-terminal PEG signal of x4-2-6 is shown at 3.55 ppm and 69.5 ppm in 1H and ^{13}C dimensions, respectively. Although significant chemical shift changes in Asn 22, Asp 23, and Asp 24 are observed, the PEG signal is not perturbed upon addition of membrane preparations.

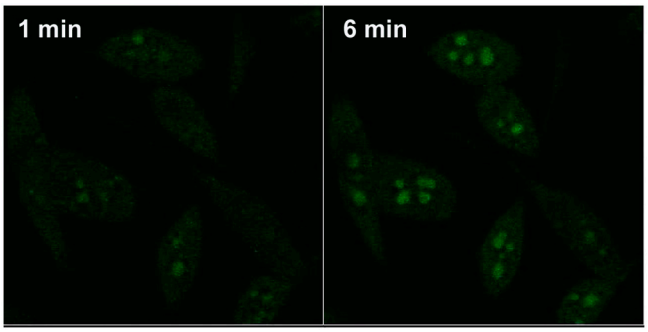

Fig. S8. Imaging of a drug release from nanoparticles upon fusion with cells. Self-assembling nanoparticles formed by X4-2-6 (0.4 mg/mL) were loaded with fluorogenic bis-imidazoacridone WMC-26(4). Molar ratio of WMC-26 to X4-2-6 was 1:200. Drug-loaded nanoparticles have been added to PC3 prostate cancer cells and imaging of drug release from nanoparticles and accumulation in the nucleus was monitored with the help of laser scanning confocal microscope. Imaging was started as soon as practical (1 min after addition of nanoparticles). The images were collected on a Zeiss LSM510 laser scanning confocal microscope using a 40 × /1.3 NA oil immersion objective lens. Fluorescence of WMC-26 (green) was excited using 488 nm band of HeNe laser and recorded using 500–550 nm emission filter and 120 μm pinhole. The time data was collected using the acquisition time of 6 s for 5 min. Image on the left is the first one in the series and was obtained 1 min after addition of nanoparticles to cells. Image on the right was obtained 6 min after addition of the nanoparticles. Rapid increase in fluorescence in the nucleus indicates drug release.

Table S1. NMR chemical shift assignments for monomeric X4-2-1 in DMSO

	HN	$H(C)_\alpha$		$H(C)_\beta$		$H(C)_{others}$
1L	not observed	3.483	(51.47)	1.367/1.347	(41.57)	γ:1.5725(23.83); δ1:0.831(23.02); δ2:0.802(21.73)
2L	8.278	4.287	(50.93)	1.365	(41.21)	γ:1.503(24.08); δ1:0.83(23.05); δ2:0.800(21.73)
3F	8.093	4.555	(53.5)	2.784/2.988	(37.07)	δ:7.168(129.01); ϵ:7.193(128.0); ζ:7.14(126.2)
4V	7.871	4.191	(57.68)	1.922	(30.77)	γ1:0.773(18.01); γ2:0.785(19.19)
5I	7.972	4.232	(56.92)	1.715	(36.41)	γ3:1.057(24.35); γ2:1.4(23.84); δ:0.773(10.98)
6T	7.785	4.202	(57.71)	3.932	(66.61)	γ:0.9666(19.7)
7L	7.753	4.494	(48.84)	1.313/1.391	(40.09)	γ:1.58(23.83); δ1:0.794(29.25); δ2:0.798(21.71)
8P	—	4.213	(59.49)	1.578/1.836	(28.74)	γ:1.712(24.42); δ3.527/3.363(46.84)
9F	7.876	4.319	(54.37)	2.781/2.921	(36.98)	δ:7.113(129.09); ϵ:7.193(128.0); ζ:7.14(126.2)
10W	7.865	4.509	(53.26)	2.988/3.106	(27.46)	δ:7.115(123.48); ϵ:7.52(118.33); ζ2:7.304(111.2); ζ3:6.944(118.27); η2:7.036 (120.82)
11A	8.043	4.308	(48.48)	1.163	(17.63)	—
12V	7.714	4.153	(57.7)	1.929	(30.61)	γ1:0.788(15.3); γ2:0.777(17.88)
13D	8.11	4.496	(49.91)	2.495/2.549	(37.07)	—
14A	8.171	4.201	(48.98)	1.215	(17.71)	—
15V	7.959	3.985	(58.79)	2.025	(29.89)	γ1:0.805(18.52); γ2:0.796(19.19)
16A	8.187	4.094	(49.01)	1.155	(17.24)	—
17N	8	4.477	(50.18)	2.476	(36.75)	δ:7.579
18W	8.029	4.316	(54.28)	2.847/3.0	(27.1)	δ:7.024(123.42); ϵ:7.409(118.0); ζ2:7.289(111.2); ζ3:76.90(118.22); η2:7.008 (120.75)
19Y	7.933	4.251	(55.02)	2.611/2.755	(36.38)	δ:6.917(130.094); ϵ:6.593(116.764)
20F	7.958	4.443	(54.29)	2.808/3.051	(37.22)	δ:7.212(129.09); ϵ:7.193(128.0); ζ:7.14(126.2)
21G	7.981	3.696	(42.09)	—	—	—
22N	8.091	4.552	(49.69)	2.394/2.551	(37.01)	δ:7.385
23D	7.695	4.129	(48.9)	2.37/2.521	(39.39)	—
24D	not observed	4.131	(48.98)	2.37/2.521	(39.39)	—